Malaysian Journal of Chemical Engineering & Technology 6(2) (2023) 152–159

**Malaysian Journal of Chemical Engineering & Technology**

*Journal Homepage: http://myjms.mohe.gov.my/index.php/mjcet*

e-ISSN: 2682-8588

# Effect of various dopants on titanium dioxide nanorod arrays: A review

[a,b] Mohd Rasydan Mustapha, [a,b] Mohd Firdaus Malek*, [c] Musa Mohamed Zahidi, [a,b] Asiah Mohd Nor, [a,b] Ruziana Mohamed, [a,b] Noor Asnida Asli, [d] Mohd Khairul Ahmad and [a,c] Mohamad Rusop Mahmood

[a]NANO-SciTech Lab (NST), Centre for Functional Materials and Nanotechnology (CFMN), Institute of Science (IOS), Universiti Teknologi MARA (UiTM), 40450 Shah Alam, Selangor, Malaysia

[b]Faculty of Applied Sciences, Universiti Teknologi MARA (UiTM), 40450 Shah Alam, Selangor, Malaysia

[c]NANO-ElecTronic Centre (NET), Faculty of Electrical Engineering, Universiti Teknologi MARA (UiTM), 40450 Shah Alam, Selangor, Malaysia

[d]Microelectronic and Nanotechnology–Shamsuddin Research Centre (MiNT-SRC), Faculty of Electrical and Electronic Engineering, Universiti Tun Hussein Onn Malaysia (UTHM), 86400, Parit Raja, Batu Pahat Johor, Malaysia

*Corresponding email: mfmalek07@uitm.edu.my; mfmalek07@gmail.com

**Abstract**

In recent years, titanium dioxide ($TiO_2$) has emerged as one of the most exceptional nanomaterials, attracting interest from experts throughout the globe. In addition to having a band gap of 3.2 eV, $TiO_2$ has outstanding optical, structural, electrical, and photocatalytic capabilities that may be used in the semiconductor industry. However, because of its weak conductivity and capacitance, $TiO_2$ has not been able to reach its full potential. In order to realise its full potential, researchers have devised a variety of methods, including hydrothermal deposition, sol-gel-assisted template deposition, chemical vapor deposition, electrochemical anodisation, hydrothermal deposition, and metal oxide doping. Doping $TiO_2$ with metal oxides has been shown to significantly enhance its properties, which may improve its qualities. The primary goal of this study is to provide an overview of various research studies on the influence of the metal oxide dopant on the final properties of titanium dioxide ($TiO_2$) nanorod arrays.

**Article Info**

*https://doi.org/10.24191/mjcet.v6i2.21827*

*Article history:*

Received date: 15 March 2023
Accepted date: 30 July 2023
Published date: 31 October 2023

*Keywords:*

Titanium dioxide
$TiO_2$
Nanorod
Metal oxide
Nanomaterials

## 1.0 Introduction

Nanotechnology is a fascinating new area of study with numerous potential applications in a variety of domains. Nanotechnology can be defined as technology on the nanoscale, which encompasses 1-100 nm, or more succinctly as atomically precise technology. It can also be defined as engineering with atomic-level precision. As a result, nanotechnology has expanded to encompass a wider range of technologies, including those with medical, catalytic, sensor, and electrical applications, as well as environmental and biological applications (Salamanca, 2005). In recent years, research into metal and metal oxide nanoparticles (NPs) have increased significantly due to the unique properties and capabilities of these materials in a variety of fields. Numerous research projects have been conducted in related disciplines, resulting in the development of various types of photovoltaic cells.

Titanium dioxide ($TiO_2$) is an inorganic semiconductor with a broad energy band of 3.2 eV (İkizler & Peker, 2016). Due to the fact that $TiO_2$ is a potential semiconductor, it possesses exceptional optical, structural, electrical, and photocatalytic properties. There are three distinct forms of $TiO_2$: anatase, brookite, and rutile. In comparison to other forms, anatase $TiO_2$ is the form of $TiO_2$ that researchers around the world are most interested in researching due to its high photocatalytic efficiency. It is a preferred material for solar cells, fuel cells, sensors, wastewater treatment, self-cleaning coatings, and disinfecting materials due to its physical and chemical stability, low toxicity, high refractive index, high reactivity, ease of

synthesis, low cost, high catalytic activity, and high energy conversion efficiency (Kusior et al., 2018). $TiO_2$ may be found in a variety of 1D, 2D, and 3D forms. When it comes to one-dimensional (1D) structures, the most common are nanowires (NWs), nanorods (NRs), and nanotubes. 1D NRs, have a high aspect ratio and are confined in the radial direction when seen from the side. Large surface areas and efficient electron transport in these structures make them favourable for reducing the recombination process to the bare minimum. $TiO_2$ NRs have clear quantum confinement, an exceptionally ordered structure, and a large explicit surface area, which allow them to significantly improve the photoinduced charge carrier separation rate and provide a high charge transport efficiency (Mokhtar et al., 2018). This is one of the reasons why $TiO_2$ NRs are well-known all over the world for their superior performance. Fig. 1 shows the field emission scanning electron microscope (FESEM) morphology of $TiO_2$ NRs.

$TiO_2$ NRs have been made by researchers all over the globe by using novel techniques such as sol-gel-assisted template, chemical vapour deposition, electrochemical anodisation, hydrothermal, and solvothermal procedures (Khanna et al., 2020). A technique known as the hydrothermal method, which has the capacity to improve the form and size of the produced nanostructure, has piqued the interest of a large number of researchers. The hydrothermal technique is a simple and uncomplicated procedure to use. It was discovered that doping $TiO_2$ with a variety of elements is an easy way to circumvent this limitation. Doping $TiO_2$ with other elements result in improved electronic properties, reduced charge recombination, increased electron transport, faster electron injection, and a band-edge shift that is more favourable (Katta et al., 2021). When doping $TiO_2$, a downward shift in the location of the conduction band (CB) leads in an increased amount of electron injection, whereas an upward shift results in a higher amount of open-circuit voltage ($V_{oc}$). Doping also plays a significant part in the modification of oxygen vacancies, which is vital in a wide range of technological applications. Doping plays a major role in several technological applications.

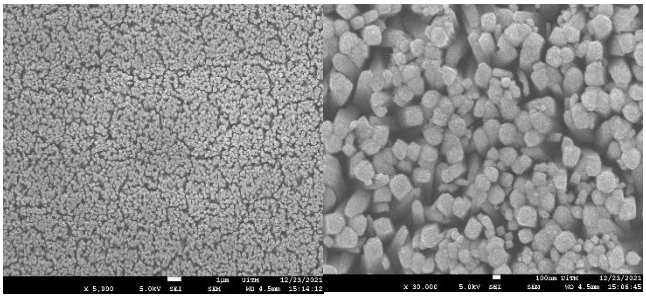

**Fig. 1**: FESEM top morphology of $TiO_2$ NRs at (a) 5k, and (b) 30k magnification

## 2.0 Synthesis of doped-titanium dioxide nanorod arrays

Doping with metal oxide is a frequent way to improve the $TiO_2$ structure. Various metal oxide can be used as dopant such niobium (Nb), calcium (Ca), yttrium (Y), gallium (Ga), antimony (Sb), and tellurium (Te) to obtain doped-metal oxide NRs.

Yang et al. (2014) used 1D rutile $TiO_2$ NRs as a photoanode for dye-sensitive solar cells (DSSCs) to investigate the influence of Nb-doping on the electrical band structure and microstructure of these NRs (Yang et al., 2014). It is directly grown on top of fluorine doped tin oxide (FTO) substrates where the NRs with varying Nb concentrations are assembled into DSSCs. Nb-doping is reported to significantly improve the energy conversion efficiency of NRs-based DSSCs by more than 70%, compared to their untreated counterparts. At the dye-NRs interface, as well as at the NRs-FTO interface, this improvement in the photon-electron conversion process may be ascribed to increased electron injection and reduced carrier recombination. Nb-doping increases the surface potential of the NRs in a positive direction, allowing electron injection from the dye sensitisers to the NRs to be facilitated. This is shown by flat band potential analysis. The researchers also discovered that the high carrier concentration of the Nb-doped NRs enhances electron tunnelling at the NRs-FTO interface, which was discovered by nanoscale conductive atomic force microscopy (c-AFM) measurements of individual NRs. According to the findings of this work, the introduction of Nb doping into the NRs changes the surface states of the NRs as well as the interface resistance between $TiO_2$ and FTO. As a result, carrier transport from the excited dye to the FTO layer is made easier by decreasing carrier recombination and increasing electron collecting efficiency.

Ca-doped $TiO_2$ nanorod arrays can be made using the one-step hydrothermal process, and the research discusses in detail the influence of Ca ions concentration on the photovoltaic conversion efficiency of dye-sensitised solar cells (Li et al., 2014). However, despite the fact that no obvious changes in the microstructure and morphology of the Ca-doped

samples were observed using the field emission scanning electron microscope and transmission electron microscope, the results of X-ray diffraction and X-ray photoelectron spectroscopy confirmed that $Ti^{4+}$ was successfully substituted with $Ca^{2+}$. The findings of the UV-Vis spectroscopy indicated that the flat band edge was positively displaced because of the Ca ions doping. Compared to the undoped electrode, the photovoltaic conversion efficiency of the dye-sensitised solar cells based on the 2% Ca-doped $TiO_2$ electrode was 43% higher, indicating that there was less chance of recombination between the dye and the electrode.

The fabrication of undoped and barium doped $TiO_2$ (Ba-$TiO_2$) nanoparticles (NPs) were made simple using the sol-gel process (Mugundan et al., 2022). The amorphous NPs were calcined at 500 degrees Celsius in order to transform them into crystalline NPs after they were manufactured. The SEM and TEM analyses of $TiO_2$ NPs following Ba doping revealed that the size of the NPs had grown. With the use of EDS and ICP-MS, the presence of Ti, O, and Ba elements in Ba-$TiO_2$ NPs was established. In the case of Ba-$TiO_2$ nanoparticles, the XRD profile revealed the existence of anatase phase and barium titanate phase. By using a BET surface area analyser, it was possible to determine the specific surface area and porosity of pure $TiO_2$ and Ba-$TiO_2$ NPs. FTIR was used to determine the functional groups of the Ba-$TiO_2$ nanoparticles. The UV-Vis spectrum was used to investigate the $E_g$ of pure $TiO_2$ and Ba-$TiO_2$ nanoparticles. According to the NLO investigations, pure $TiO_2$ NPs had a greater second harmonic generation (SHG) efficiency when compared to Ba-$TiO_2$ NPs under the same conditions. In this study, the photocatalytic activity of pure $TiO_2$ and Ba-$TiO_2$ nanoparticles were examined in relation to the degradation of methylene blue (MB) dye when exposed to sunlight. The TOC analyser was used to investigate the mineralisation of methylene blue dye.

A simple one-step hydrothermal process was used to create Y-doped $TiO_2$ nanorod arrays, which were then effectively used as the photoanode in photovoltaic solar cells (Lv et al., 2018). The rutile structure of $TiO_2$ was preserved after Y doping, and the strength of several diffraction peaks was increased, suggesting that Y-doped $TiO_2$ NRs crystallised more efficiently. Doping with Y also raised the electron concentration, which resulted in an even greater increase in electron conductivity. Furthermore, the flat band edge of Y-doped NRs moves positively, which contributes to the improvement of the electron-injection efficiency, which in turn results in a rise in the current density of the device. It was discovered that the PSC based on Y-doped $TiO_2$ could achieve an overall power conversion efficiency of 7.95%. When compared to the non-doped counterpart, this represents a 24% gain in performance. The increased electron injection and transfer efficiency generated by a positive shift in $V_{fb}$, as well as a decrease in charge recombination, were described to the improve of performance. The findings of this work pave the way for the enhancement of photocurrent density in perovskite solar cells by the use of element doping.

$TiO_2$ with varied morphologies were developed and synthesised with ease by manipulating the seeding concentration and subsequent nitridation, which were done in a simple and straightforward manner (Su et al., 2020). While it is possible to generate $TiO_2$ microflowers in the lack of $TiO_2$ seeds, it is also possible to form $TiO_2$ nanorod arrays in the presence of $TiO_2$ seeds. A variety of $TiO_2$ seeding concentrations were used in the preparation procedure in order to determine the most favourable synthesis conditions for $TiO_2$ production. Consequently, N-$TiO_{2-3}$ synthesised using 0.2 g L1 $TiO_2$ seeds exhibits higher areal capacitance than N-$TiO_{2-3}$ synthesised using 0.2 g L1 $TiO_2$ seeds, which is attributed to the rapid charge transfer and improved hybrid structure of free-standing NRs and nanoflowers. The highest areal capacitance of the optimised N-$TiO_{2-3}$ electrode was 177.1 mF $cm^2$, which is much greater than the maximum areal capacitance of the no seeding sample (16 mF $cm^2$). Through the manipulation of the concentration of the seed solution, this approach offers a broad way for improving the areal capacitance of nanomaterials.

They reported the $TiO_2$ NAs with varying molar ratios of zinc doping were employed as electron transport layers (ETLs) for carbon-based perovskite solar cells with improved photovoltaic performance, and the ETLs were shown to be effective (Lv et al., 2021). By using a one-step hydrothermal process, the zinc-doped $TiO_2$ NAs were produced directly on the conductive fluorine-doped tin oxide (FTO) substrate using zinc-doped $TiO_2$ NAs. It can be seen from the XRD patterns that the addition of Zn dopant improves the vertical growth orientation of $TiO_2$ NAs as well as the crystallinity of perovskite films. The measurements of the space-charge-limited current (SCLC) demonstrate that Zn-doped $TiO_2$ NAs have better electrical conductivity and lower trap-state density than

pure $TiO_2$, resulting in an increase in $J_{sc}$. The Mott-Schottky measurement determines the location of the conduction band, which implies more electron injection into the perovskite layer, resulting in an improvement in the $J_{sc}$ of the material. By optimising the zinc doping concentration, the PCE increased from 12.99% to 14.45%, a significant improvement (2.5 mol %). Furthermore, according to stability tests conducted over a 30-day period, the best-performing cell without encapsulation retains 85% of its initial efficiency.

A straightforward hydrothermal approach was used to create Ce-doped $TiO_2$ NRs (Chen et al., 2021). The length and diameter of Ce doped NRs, as determined by FESEM, are around 500 nm and 80 nm, respectively (Chen et al., 2021). The XRD results show that $Ce^{4+}$ has taken the position of $Ti^{4+}$ in the crystal lattice without affecting the $TiO_2$ crystal structure at all. The doping of $Ce^{4+}$ in $TiO_2$ NRs, as shown by SEM, reduces the grain size of the NRs. The effective integration of Ce ions is shown by the XRD and EDS patterns. The UV-Vis absorption spectra and PL emission spectra of the down-conversion centre $Ce^{4+}$ ions demonstrate that the ions can effectively use ultraviolet light and that the perovskite functional layer can enhance the light-harvesting ability of the perovskite functional layer to the ultraviolet region. The photoelectric performance varies depending on the concentration of Ce doping used. When the Ce-doping concentration is 0.05 (Ce: Ti molar ratio), the hole-transport-free and carbon electrode-based perovskite solar cells achieve the greatest performance, the hole-transport-free and carbon electrode-based perovskite solar cells reach the highest performance. The power conversion efficiency (PCE) of the optimised Ce-doped device was 10.1%, a 24.6% improvement over the efficiency of the undoped device. The dark current density and hysteresis effect of the Ce-doped cells are both less than those of the undoped cells, indicating that they are more efficient. Upon Ce doping, the band gap of $TiO_2$ is increased from 2.92 to 3.00 eV, and the flat band potential is de-shifted by 50 mV to the negative side, leading to a higher Fermi level and a reduction in the surface defect density, all of which contribute to boosting the $V_{oc}$ of the PSCs. The electron lifespan is extended by the Ce (0.05)-$TiO_2$ device, as seen by the $V_{oc}$ decay curve. According to the results of the impedance study, more carriers are created. Additionally, the UV stability has been greatly increased. Even after 12 hours of exposure to light at room temperature in an optimised Ce-doped device, PCE maintains 90% of its original value. The value of the undoped gadget, on the other hand, declines to 55% of its starting value.

Spin coating was used to create high grade nanocrystalline Fe doped $TiO_2$ films (Komaraiah et al., 2019). Research on the structural, optical, and photocatalytic activity (PCA) effects of Fe doping has been conducted. $TiO_2$ crystallite size shrank as Fe doping concentrations increased. Table 1 shows by using HRTEM images, it was determined that the average particle size of 1% and 7% Fe doped $TiO_2$ films were 14 nm and 8 nm, respectively. As Fe doping concentration increased, the crystallite size decreased, and the Raman blue shift was ascribed to it. The bandgap of $TiO_2$ is reduced from 3.32 eV to 2.57 eV when the concentration of Fe dopant is increased. As $Fe^{3+}$ is added to doped $TiO_2$ thin films, the PL emission intensity drops. An increased PCA was attributed to Fe-$TiO_2$ films because of their large specific surface area, decreased bandgap energy, and increased absorption of visible light. MB dye photodegradation maximised when exposed to light via, fluorine doped-tin oxide sample 7, FTO7 film. The PCA of $TiO_2$ thin films shows that the photodegradation efficiencies for the disintegration of MB under visible light irradiation decrease as the content of Fe-precursors increases.

Sol-gel spin coating successfully applied $Ag^+$ doped $TiO_2$ thin films on glass substrates (Komaraiah et al., 2020). Table 1 states the average Ag–$TiO_2$ crystallite size was 6.2 to 18.0 nm. Ag doping reduced crystallite size. TEM images show that pure $TiO_2$ is 23.8 nm and $Ag^+$ doped $TiO_2$ is 11.6 nm. Due to a decrease in crystallite size, the vibrational Raman modes in Ag-doped titania films moved towards higher energy. Increasing Ag-precursor concentration decreases $TiO_2$ bandgap from 3.32 to 2.75 eV. The high PCA during visible light irradiation is due to oxygen vacancies and $Ti^{3+}$ sites in Ag–$TiO_2$, as shown by EPR spectra. Silver ion doping reduces luminescence emission. Silver-doped titanium dioxide at 5%, ATO5 film causes dye degradation. Degradation efficiencies rise with $Ag^+$ doping concentration, reaching a maximum at 5% Ag and decreasing at higher concentrations for visible light dye breakdown. Smaller crystallite and particle size, narrow bandgap, and optimum doping concentration may improve degradation efficiency. Given their good PCA and easy deposition, coated Ag-$TiO_2$ films may have photocatalytic applications.

Moreover, the spin coating process was used to make the KI-doped $TiO_2$ film, and the optical

absorbance of the $TiO_2$ film was increased by doping alkali halide (Shanthi et al., 2022). The presence of an anatase phase structure in the grown film was shown by Raman spectrum and X-ray diffraction studies, respectively. A shift from the ultraviolet to the visible range was observed using UV-Vis spectroscopy, and an increase in particle size of the anatase crystal resulted in a lower energy band gap when measured using FESEM. Both studies demonstrate that the optical absorbance of the alkali halide doped film is ensured by the alkali halide doped film. Energy dispersive X-ray spectroscopy (E-DAX) was used to demonstrate the presence of a dopant, and the created film was confirmed to be free of contaminants after being processed. Thus, the doped film may be employed as an excellent optical absorber for photovoltaic cells as a consequence of its enhanced absorption properties.

An acidic sol-gel technique was used to fabricate both pure $TiO_2$ and $TiO_2$ nanoparticles that had been doped with varying amounts of Zn and Mg (Javed et al., 2022). Table 1 states pure samples were calcined at 400 °C for 4 hours. Pure $TiO_2$, Mg-doped $TiO_2$, and ZnO-doped $TiO_2$ were examined for their surface morphology, crystal dimensions, bandgap size, and visible light absorption. X-ray diffraction analysis confirmed the presence of the anatase phase in both undoped $TiO_2$ and Zn/Mg-doped $TiO_2$ nanoparticles. According to the scanning electron micrographs, both pure $TiO_2$ and Zn/Mg-doped $TiO_2$ nanoparticles were aggregated into particles of about the same size and shape during preparation. Pure $TiO_2$ was found to have a mean particle size of 5 nm, whereas Mg-doped $TiO_2$ nanoparticles were found to be 30 nm and Zn-doped $TiO_2$ nanoparticles were found $TiO_2$ has a wide PL spectrum because of its indirect energy bandgap, which can be seen in UV-Vis spectra as an expansion of the valence band. The data also shows that the peak intensity increases with Mg doping due to a greater recombination rate. ZnO doping, however, was crucial in preventing this narrowing. By using the sol-gel spin coating method, it was possible to create $TiO_2$ thin films that were doped with varying concentrations of $Fe^{3+}$ (Carotta et al., 1999). Analysis using X-ray diffraction and Raman spectroscopy demonstrate that, depending on their concentration, the Fe ions either restrict the crystallisation process or appear to stabilise the amorphous phase of the $TiO_2$ material. As stated in Table 1, the concentration of Fe in thin films was increased, the edge of absorption moved farther out to longer wavelengths, moving from 356 to 416 nm. The band gap of $TiO_2$ may be shrunken via Fe-doping in the material. The photocatalytic activity in the visible spectrum functions more effectively as a result of this impact. The crystallinity of the material dropped as the amount of $Fe^{3+}$ in it climbed from 0 to 20%. Despite the addition of $Fe^{3+}$ to a concentration of 20%, the amorphous condition of the $TiO_2$ thin film did not change. The grain size determined from the XRD patterns ranges anywhere from 29.3 to 22.6 nm.

Hydrothermal synthesis has been used to produce $TiO_2$ as well as N-GO-doped $TiO_2$ (M. Sharma and Nihal, 2019) The FESEM and XRD techniques have been used so that the structure may be characterised. The NRs type morphology is seen for $TiO_2$ by FESEM, but the spherical morphology is observed for N-GO doped $TiO_2$. Techniques such as FTIR, UV-Vis, and PL spectroscopy are used in order to investigate the optical characteristics. Referring to Table 1, there is a red shift in energy in the band gap of both pure $TiO_2$ and N-GO-doped $TiO_2$. The current-voltage (I-V) characteristics have been used in carrying out the electrical measurements. The electrochemical approach was used to compute the value of the specific capacitance, and the results turned out to be 16.41 $Fg^{-1}$ for $TiO_2$ and 121.40 $Fg^{-1}$ for N-GO doped $TiO_2$, respectively.

Next, they investigated the photovoltaic performance of dye-sensitised solar cells based on undoped and Sr-doped $TiO_2$ photoanodes with $TiO_2$ scattering layers and $TiCl_4$ treatment, in order to summarise their findings (Rajamanickam and Ramachandran, 2020). With the addition of Sr doping and treatment with $TiCl_4$, the efficiency increased from 2.74% for the bare undoped $TiO_2$ photoanode to 9.6% for the finished product. Several variables have contributed to the greater efficiency. The dielectric, electrochemical impedance spectroscopy (EIS), and incident photon-to-current efficiency (IPCE) tests on the Sr-doped $TiO_2$ sample reveal that the material exhibits rapid charge separation. Furthermore, IPCE measurements revealed that TiCl4-treated and scattering layer-coated $TiO_2$ photoanodes had high photon energy for charge transport as well as decreased charge recombination. Aside from that, the TiCl4-treated photoanode has the lowest charge transfer resistance, which results in a high photocurrent density and efficiency in the Sr-doped $TiO_2$ photoanodes.

**Table 1:** Comparison on the preparation of element doped $TiO_2$ NRAs by various research groups

| No. | Starting Materials | Deposition Method | Parameter Involved | Findings | Ref. |
|---|---|---|---|---|---|
| 1. | • Titanium isopropoxide<br>• Chloride of iron (III)<br>• Isopropanol<br>• Acetic acid | Sol-gel spin coating technique | • Iron (5%, 10% and 20%) | • $Fe^{3+}$ concentration from 0% to 20% reduced crystallinity<br>• TiO2 thin film remained amorphous after 20% $Fe^{3+}$ addition<br>• Grain sizes between 29.3 and 22.6 nm<br>• Increasing $Fe^{3+}$ lowered the optical bandgap | (Carotta et al., 1999) |
| 2. | • Ammonia ($NH_3$)<br>• Sodium Hydroxide<br>• Titanium dioxide | Hydrothermal | • Pristine $TiO_2$ and 0.2g of N-GO Doped $TiO_2$ | • $TiO_2$ and N-GO Doped $TiO_2$ band gap energy display red shift.<br>• Specific capacitance values for $TiO_2$ and N-GO doped $TiO_2$ were 16.41 $Fg^{-1}$ and 121.40 $Fg^{-1}$, respectively. | (Sharma & Nihal, 2019) |
| 3. | • Titanium(IV) propoxide<br>• Acetylacetone | Sol-gel spin coating technique | • Iron (0, 1, 3, 5, 7 and 10%) | • The average particle size of 1% and 7% Fe-doped $TiO_2$ films was determined to be 14 and 8 nm.<br>• As Fe doping concentration increased, the Raman blue shift was seen. | (Komaraiah et al 2019) |
| 4. | • Titanium tetra isopropoxide<br>• Magnesium chloride<br>• Zinc nitrate hexahydrate<br>• Ethanol<br>• Deionized water | Facile sol–gel technique | • Zinc (0.25 M, 0.5 M, and 1 M)<br>• Magnesium (1 M and 2 M) | • Good thermal stability and fewer surface flaws than ZnO-doped $TiO_2$.<br>• Mg-doped $TiO_2$ nanoparticles limit recombination processes to display visible absorption. | (Javed et al., 2022) |
| 5. | • Titanium(IV) propoxide<br>• Acetyl acetone<br>• Nitric acid | Sol-gel spin coating technique | • Silver concentration (0, 1, 3, 5, 7, and 10%) | • $Ag^{+}$ doped $TiO_2$ films outperformed undoped $TiO_2$ in photocatalysis.<br>• PL emission efficiency was poor in Ag-doped $TiO_2$ compared to $TiO_2$ thin film.<br>• The Raman bands showed anatase phase development. | (Komaraiah et al., 2020) |

## 3.0 Conclusions

This work gives an overview of the metal oxide element that is employed in the manufacture of $TiO_2$ NRs, as well as the influence of doping on the characteristics of the NRs. There are several more techniques that may be employed to improve the characteristics of $TiO_2$ NRs. Because of the unique qualities that $TiO_2$ material has, it has the potential to be the optimal solution with a great deal of promise in a broad range of applications. Since the usage of dopants have a substantial impact on the characteristics of $TiO_2$ NRs, this will be a fantastic chance to learn about the new technology that it delivers. As a result, more research is necessary to improve the properties of $TiO_2$ NRs and to maximise their potential for use in larger-scale applications. According to the findings of this research, $TiO_2$ NRs have the potential to become one of the most important semiconductor materials, as well as having additional uses.

## Contribution statement

**Mohd Firdaus Malek, Mohd Khairul Ahmad & Mohamad Rusop Mahmood:** Conceptualisation and supervision; **Mohd Rasydan Mustapha, Mohd Firdaus Malek and Musa Mohamed Zahidi:** Methodology; **Mohd Rasydan Mustapha & Mohd Firdaus Malek:** Formal analysis and investigation; **Mohd Firdaus Malek, Asiah Mohd Nor, Mohd Khairul Ahmad & Mohamad Rusop Mahmood:** Resources; **Mohd Rasydan Mustapha & Mohd Firdaus Malek:** Writing-original draft; **Musa Mohamed Zahidi, Asiah Mohd Nor, Ruziana Mohamed, Noor Asnida Asli:** Writing-review and editing; **Mohd Firdaus Malek & Mohamad Rusop Mahmood:** Project administration.

## Conflict of interest

The authors declare that they have no known competing financial interests or personal relationships that could have appeared to influence the work reported in this paper.

## Acknowledgement

This work was supported by Grant No. 600-RMC/GPM LPHD 5/3 (072/2021). The authors would like to thank the Research Management Centre (RMC), Universiti Teknologi MARA (UiTM), and Ministry of Higher Education Ministry (MoHE), Malaysia for the financial support. The authors thank Ts. Irmaizatussyehdany Buniyamin (Senior Research Officer), Mr. Salifairus Mohammad Jafar (Senior Science Officer), Mr. Mohd Azlan Jaafar (assistant engineer), Mr. Suhaimi Ahmad (assistant engineer) and Mr. Muhamad Faizal Abd Halim (Assistant Research Officer) for their kind support on this research.

## References

Carotta, M.C., Ferroni, M., Gnani, D., Guidi, V., Merli, M., Martinelli, G., Casale, M.C., Notaro, M. (1999). Nanostructured pure and Nb-doped $TiO_2$ as thick film gas sensors for environmental monitoring. *Sensors and Actuators, B: Chemical*, *58*(1–3), 310–317. https://doi.org/10.1016/S0925-4005(99)00148-3

Chen, K., Zhang, H., Tong, H., Wang, L., Tao, L., Wang, K., Zhang, Y., & Zhou, X. (2021). Down-conversion Ce-doped $TiO_2$ nanorod arrays and commercial available carbon-based perovskite solar cells: Improved performance and UV photostability. *International Journal of Hydrogen Energy*, *46*(7), 5677–5688. https://doi.org/10.1016/j.ijhydene.2020.11.074

Ikizler, B., & Peker, S. M. (2016). Synthesis of $TiO_2$ coated ZnO nanorod arrays and their stability in photocatalytic flow reactors. *Thin Solid Films*, *605*, 232–242. https://doi.org/10.1016/j.tsf.2015.11.083

Javed, H.M.A., Adnan, M., Qureshi, A.A., Javed, S., Adeel, M., Akram, M.A., Shahid, M., Ahmad, M.I., Afzaal, M., Abd-Rabboh, H.S.M., Arif, M. (2022). Morphological, structural, thermal, and optical properties of Zn/Mg-doped $TiO_2$ nanostructures for optoelectronic applications. *Optics & Laser Technology*, *146*, 107566. https://doi.org/10.1016/j.optlastec.2021.107566.

Katta, V. S., Das, A., Dileep K., R., Cilaveni, G., Pulipaka, S., Veerappan, G., Ramasamy, E., Meduri, P., Asthana, S., Melepurath, D., & Raavi, S. S. K. (2021). Vacancies induced enhancement in neodymium doped titania photoanodes based sensitized solar cells and photo-electrochemical cells. *Solar Energy Materials and Solar Cells*, *220*, 110843. https://doi.org/10.1016/j.solmat.2020.110843

Khanna, S., Utsav, Patel, R., Marathey, P., Chaudari, R., Vora, J., Banerjee, R., Ray, A., & Mukhopadhyay, I. (2019). Growth of titanium dioxide nanorod over shape memory material using chemical vapor deposition for energy conversion application. *Materials Today: Proceedings*, *28*, 475–479. https://doi.org/10.1016/j.matpr.2019.10.035

Komaraiah, D., Radha, E., Sivakumar, J., Ramana Reddy, M. V., & Sayanna, R. (2020). Photoluminescence and photocatalytic activity of spin coated $Ag^+$ doped anatase $TiO_2$ thin films. *Optical Materials*, *108*, 110401. https://doi.org/10.1016/j.optmat.2020.110401

Komaraiah, D., Radha, E., Sivakumar, J., Ramana Reddy, M.V., Sayanna, R. (2019). Structural, optical properties and photocatalytic activity of $Fe^{3+}$ doped $TiO_2$ thin films deposited by sol-gel spin coating Author links open overlay panel. *Surfaces and Interfaces*, *17*, 100368. https://doi.org/10.1016/j.surfin.2019.100368

Kusior, A., Banas, J., Trenczek-Zajac, A., Zubrzycka, P., Micek-Ilnicka, A., & Radecka, M. (2018). Structural properties of $TiO_2$ nanomaterials. *Journal of Molecular Structure*, *1157*, 327–336. https://doi.org/10.1016/j.molstruc.2017.12.064

Li, W., Yang, J., Zhang, J., Gao, S., Luo, Y., & Liu, M. (2014). Improve photovoltaic performance of titanium dioxide nanorods based dye-sensitized solar cells by Ca-doping. *Materials Research Bulletin*, *57*, 177–183. https://doi.org/10.1016/j.materresbull.2014.05.034

Lv, Y., Li, Y., Sun, H., Guo, Y., Li, Y., Tan, J., & Zhou, X. (2018). Yttrium-doped $TiO_2$ nanorod arrays and application in perovskite solar cells for enhanced photocurrent density. *Thin Solid Films*, *651*, 117–123. https://doi.org/10.1016/j.tsf.2018.02.022

Lv, Y., Tong, H., Cai, W., Zhang, Z., Chen, H., & Zhou, X. (2021). Boosting the efficiency of commercial available carbon-based perovskite solar cells using Zinc-doped $TiO_2$ nanorod arrays as electron transport layer. *Journal of Alloys and Compounds*, *851*, 156785. https://doi.org/10.1016/j.jallcom.2020.156785

Mokhtar, S. M., Ahmad, M. K., Soon, C. F., Nafarizal, N., Faridah, A. B., Suriani, A. B., Mamat, M. H., Shimomura, M., & Murakami, K. (2018). Fabrication and characterization of rutile-phased titanium dioxide ($TiO_2$) nanorods array with various reaction times using one step hydrothermal method. *Optik*, *154*, 510–515. https://doi.org/10.1016/j.ijleo.2017.10.091

Mugundan, S., Praveen, P., Sridhar, S., Prabu, S., Lawrence Mary K., Ubaidullah, M., Shaikh, S. F., Kanagesan, S. (2022). Sol-gel synthesized barium doped $TiO_2$ nanoparticles for solar photocatalytic application. *Inorganic Chemistry Communications*, *139*, 109340. https://doi.org/10.1016/j.inoche.2022.109340

Rajamanickam, N., & Ramachandran, K. (2020). Improved photovoltaic performance in nano $TiO_2$ based dye sensitized solar cells: Effect of $TiCl_4$ treatment and Sr doping. *Journal of Colloid and Interface Science*, *580*, 407–418. https://doi.org/10.1016/j.jcis.2020.07.041

Salamanca-Buentello, F., Persad, D. L., Court, E. B., Martin, D. K., Daar, A. S., & Singer, P. A. (2005). Nanotechnology and the developing world. *PLoS Medicine*, *2*(5), 0383–0386. https://doi.org/10.1371/journal.pmed.0020097

Shanthi, J., Aishwarya, S., & Swathi, R. (2020). Enhanced optical & structural properties by potassium iodide doping on spin coated $TiO_2$ thin films. *Chemical Data Collections*, *29*, 100494. https://doi.org/10.1016/j.cdc.2020.100494

Sharma, M., & Nihal. (2020). Effect of N-doped graphene on optical, electrical, and electrochemical properties of hydrothermally synthesized $TiO_2$ nanocomposite. *Materials Today: Proceedings*, *26*, 3390–3396. https://doi.org/10.1016/j.matpr.2019.11.022

Su, X., He, Q., Yang, Y. e., Cheng, G., Dang, D., & Yu, L. (2021). Free-standing nitrogen-doped TiO2 nanorod arrays with enhanced capacitive capability for supercapacitors. *Diamond and Related Materials*, *114*(October 2020), 108168. https://doi.org/10.1016/j.diamond.2020.108168

Yang, M., Ding, B., & Lee, J. K. (2014). Surface electrochemical properties of niobium-doped titanium dioxide nanorods and their effect on carrier collection efficiency of dye sensitized solar cells. *Journal of Power Sources*, *245*, 301–307. https://doi.org/10.1016/j.jpowsour.2013.06.016